TÜBİTAK

Turkish Journal of Chemistry

http://journals.tubitak.gov.tr/chem/

Research Article

Turk J Chem
(2020) 44: 1463-1470

doi:10.3906/kim-2005-78

Synthesis and structural analysis of nonstoichiometric ternary fulleride $K_{1.5}Ba_{0.25}CsC_{60}$

Havva Esma OKUR KUTAY*
Department of Chemistry, Faculty of Engineering and Natural Sciences, Bursa Technical University, Bursa, Turkey

Received: 30.05.2020 • **Accepted/Published Online:** 27.07.2020 • **Final Version:** 16.12.2020

Abstract: The existence of cation-vacancy sites in fullerides might lead to long-range ordering and generate a new vacancy-ordered superstructure. The purpose of this work is to search whether or not long-range ordering of vacant tetrahedral sites, namely superstructure emerges in nonstoichiometric $K_{1.5}Ba_{0.25}CsC_{60}$ fulleride. Therefore, $K_{1.5}Ba_{0.25}CsC_{60}$ with cation-vacancy sites is synthesized using a precursor method to avoid inadequate stoichiometry control and formation of impurity phases within the target composition. For this purpose, first, phase-pure K_6C_{60}, Ba_6C_{60} and Cs_6C_{60} precursors are synthesized. Stoichiometric quantities of these precursors are used for further reaction with C_{60} to afford $K_{1.5}Ba_{0.25}CsC_{60}$. Rietveld analysis of the high-resolution synchrotron X-ray powder diffraction data of the precursors and $K_{1.5}Ba_{0.25}CsC_{60}$ confirms that K_6C_{60}, Ba_6C_{60} and Cs_6C_{60} are single-phase and they crystallize in a body-centered-cubic structure ($Im\bar{3}$) as reported in the literature. The analysis also shows that $K_{1.5}Ba_{0.25}CsC_{60}$ phase can be perfectly modeled using a face-centered cubic structure. No new peaks appear which could have implied the appearance of a superstructure. This suggests that there is no long-range ordered arrangement of vacant tetrahedral sites in $K_{1.5}Ba_{0.25}CsC_{60}$.

Key words: Cation-vacancy, solid-state synthesis, A_6C_{60}, nonstoichiometric fullerides

1. Introduction

The intercalated products of fullerides display unique structural, magnetic, and electronic properties which depend on the amount, size, and nature of the intercalated species, and the synthetic route employed for the intercalation of dopant into solid C_{60}, i.e. exohedral doping [1]. Synthetic efforts have been essentially focused on the synthesis of alkali fullerides with stoichiometries A_xC_{60} (A = alkali metal, $1 \le x \le 12$, *e.g.* RbC_{60}, $Li_{12}C_{60}$), due to their novel electronic properties. For instance, the observation of metallic behavior in alkali metal intercalated C_{60} films at 300 K [2] was followed by the discovery of superconductivity for the first time in an alkali fulleride K_3C_{60} with a transition temperature, T_c, of 18 K [3], where superconducting phase is a face-centered-cubic (fcc) structure [4,5]. This led to the discovery of new A_3C_{60} superconductors through varying the interfullerene separation (*e.g.* Rb_3C_{60} with a T_c of 28 K [6] and 30 K [4], Rb_2CsC_{60} and $RbCs_2C_{60}$ with a T_c of 31 K and 33 K, respectively [7], fcc Cs_3C_{60} with a maximum T_c of 35 K at ~7 kbar [8] and fcc $Rb_xCs_{3-x}C_{60}$ ($0.35 \le x \le 2$) with T_c varying between 25.9 K and 32.9 K at ambient pressure [9]). Since then, extensive research has been carried out on fcc A_3C_{60} and $A_xCs_{3-x}C_{60}$ fullerides to discover superconductors with higher T_c and understand their molecular electronic structure [8–12]. Current understanding proves that the A_3C_{60} superconducting fullerides belong to the family of unconventional superconductivity where electron correlations play an important role for the pairing mechanism [8–11, and 13–18]. Besides that, molecular electronic structure [9,19,20] and cation specific effects [12] are crucially important in producing the unconventional superconductivity in the A_3C_{60} family.

Upon exohedral doping of solid C_{60}, the dopant occupies interstitial lattice positions of the solid C_{60} and provides electrons to the host C_{60} molecules, creating C_{60}^{n-} anions [1]. The charge transfer alters the properties of C_{60} (e.g. inducing metallicity and superconductivity) and has thus received the most attention. In the A_3C_{60} family, intercalation of three alkali leads to a half-filled t_{1u} band and hence a metallic behavior, excluding fcc Cs_3C_{60} [8]. The superconducting phase of the A_3C_{60} fullerides adopts the fcc structure where all tetrahedral (T_d) and octahedral (O_h) holes are entirely occupied by the alkali cations [21]. In fcc A_3C_{60} structure, there are two T_d cavities (r = 1.12 Å) and one O_h (r = 2.06 Å) per C_{60} unit. As the T_d cavity is smaller than the O_h one, the size of the alkali cation occupying the T_d site instead of the O_h one will determine the degree of lattice expansion; therefore, the volume of the A_3C_{60} fullerides can be changed systematically through substituting the alkali metals with larger ones.

* Correspondence: esma.okur@btu.edu.tr

Various synthetic routes have been developed to prepare A_xC_{60} fullerides. The most common and effective one is the 'solid-state direct reaction method' where solid C_{60} is exposed to vapor of the alkali metal which then disperses into the C_{60} acceptor molecules at temperatures of ~100–410 °C. All the A_xC_{60} and $A_xA'_{3-x}C_{60}$ compounds, except Cs_3C_{60} [8,10], can be synthesized with this method [1]. The A_6C_{60} fullerides can be synthesized using the direct reaction method and used later as precursors for further reaction with C_{60} to obtain target $A_xCs_{3-x}C_{60}$ compounds. The precursor method offers a significant benefit compared to the direct synthesis method because fine A_6C_{60} powders enable better stoichiometry control of the desired compound. The saturated A_6C_{60} compounds can also be prepared by a vapor-transport method [22]. In this study, direct reaction and vapor-transport methods were used to synthesize the K_6C_{60}/Ba_6C_{60} and Cs_6C_{60} precursors, respectively, which were later reacted with C_{60} to afford the target composition.

Besides the exploration of cation related effects on the structural and electronic properties of fullerides, the effects of cation-vacancy can be investigated as well. For example, tetrahedral rare-earth metal vacancies in $Sm_{2.75}C_{60}$ and $Yb_{2.75}C_{60}$ exhibit long-range ordering of tetrahedral vacancies, generating a superstructure [23,24]. Such structural response to tetrahedral vacancy could be established in fcc $A_xCs_{3-x}C_{60}$ fullerides, resulting in a different structure to the fcc. For such an exploration, in this work, $[\,]_{0.25}K_{1.5}Ba_{0.25}CsC_{60}$ —where [ ] represents vacant tetrahedral sites of the fcc structure — was synthesized using stoichiometric quantities of single phase, fine, black colored K_6C_{60}, $Ba_6C_{60,}$ and Cs_6C_{60} powders together with C_{60} as starting materials. Here, an easy method for the synthesis of nonstoichiometric $K_{1.5}Ba_{0.25}CsC_{60}$ is presented together with the results of Rietveld analysis of high-resolution synchrotron X-ray powder diffraction data collected at ambient conditions for the structural investigation.

2. Materials and methods

2.1. Synthetic route

All sample operations were performed in an argon-filled glove box (MBraun MB 200B, H_2O and O_2 < 0.1 ppm) due to the extreme air- and moisture-sensitivity of reactants. As purchased pristine C_{60} (MER corporation, 99.9%) was sublimed prior to synthesis. Solid C_{60} (~500–600 mg) were first ground and then loaded in a quartz ampoule with a separating striction. This was followed by degassing for 3–4 h in a dynamic vacuum of 10^{-4}–10^{-5} mbar. The sublimation process was undertaken in a tube furnace at 550 °C (ramping 10 °C/min) under dynamic vacuum. As soon as the sublimation ended, the sublimed C_{60} was transferred to the glove box for later use. A Swagelok fitting with J. Young tap (Sigma-Aldrich Corp., St. Louis, MO, USA) was always used while the samples within the tubes were removed or introduced from or into the glove box. Each cycle of annealing of the intermediate and final products was ended through allowing the furnace to cool down to room temperature with a rate of 5 °C/min. Once each annealing cycle was complete, these products were ground using a pestle and mortar to improve crystallinity.

Synthesis of K_6C_{60}

Stoichiometric amount of K metal was placed in a 5 mm diameter Ta cell and then stoichiometric amount of sublimed C_{60} was introduced onto K in the cell. The cell was then located in a glass tube enclosed with a Swagelok fitting, removed from the glove box, evacuated for 30 min before sealing under 350 mbar of He gas pressure. The sealed sample within the glass tube was placed vertically in a box furnace and heated to 250 °C with a rate of 5 °C/min, followed by another 20 h annealing and cooling to ambient temperature with the same rate as heating. After the initial annealing was completed, the product was transferred to the glove box, removed from the reaction vessel, and ground. The ground product was then pressed into a pellet, introduced into a Ta holder for further period of 2 days annealing at 300 °C to increase the crystallinity.

Synthesis of Cs_6C_{60}

Phase-pure Cs_6C_{60} was synthesized by a vapor transport method using a ~2.3× excess amount of Cs. The solid C_{60} was first placed into a glass tube with a striction. The cesium metal was inserted in a small glass capsule (~7 mm diameter) which was lowered in the glass tube down to where the striction was. The tube enclosed with a Swagelok fitting was removed from the glove box and evacuated for 30 min before sealing under ~400 mbar of He gas pressure. A 3-zone horizontal tube furnace was used in order to create a temperature gradient between Cs and C_{60} for vapor transport. The zone where Cs locates was ramped to 350 °C from room temperature with a rate of 2 °C/min and held there for 3 days. Simultaneously, the zone where C_{60} locates was ramped to 330 °C (2 °C/min) for transportation of vapor from the Cs to C_{60} zone. Before the product was cooled down to ambient temperature, the temperature gradient was reversed to get rid of any undoped Cs from the freshly formed Cs_6C_{60}. Once the cooling was complete, the product was removed from the glass tube, ground thoroughly, pelletized, and located in a Ta cell with tightened screw ends which was then sealed under He, after evacuation under dynamic vacuum, and annealed at 350 °C for another 3 days to increase the crystallinity.

Synthesis of Ba_6C_{60}

Prior to synthesis, in order to obtain oxide-free barium powder, the oxidized surface of a barium rod was first removed by filing. These initial filings were discarded, and a new diamond file was used to exfoliate the required mass of clean fine powder. Once the clean fine powder was obtained, stoichiometric amount of barium powder and C_{60} were mixed and ground using a mortar and pestle, and then pressed into a pellet. The reaction mixture was loaded into a Ta holder which was placed a 15 mm diameter quartz tube then evacuated for 30 min before sealing under 500 mbar of He gas pressure. The sealed mixture was heated inside a muffle furnace using the following thermal protocol: from ambient temperature to 550 °C; held for 1 h; to 650 °C; held for 13 h; to 700 °C; held for 4 h; to 720 °C; held for 18 h. The ramping rate between each step of heating was 5 °C/min. After cooling to room temperature, the product was removed from the reaction vessel, ground, and finally pressed into a pellet and inserted into the same Ta holder for reannealing at 740 °C for 16 h.

Synthesis of the target compound $K_{1.5}Ba_{0.25}CsC_{60}$

$K_{1.5}Ba_{0.25}CsC_{60}$ was prepared by a solid state synthetic route according to the following stoichiometric equation describing the ideal reaction: $6K_6C_{60} + 4Cs_6C_{60} + Ba_6C_{60} + 13C_{60} \rightarrow 24K_{1.5}Ba_{0.25}CsC_{60}$. Stoichiometric amounts of K_6C_{60}, Ba_6C_{60}, Cs_6C_{60}, and sublimed C_{60} precursors were mixed and ground thoroughly. The ground mixture was pelletized, introduced into a Ta cell with tightened screw ends which was then placed in a quartz tube, and evacuated for 30 min before sealing under 450 mbar of He gas pressure. The sealed pellet was then positioned in a muffle furnace at room temperature and heated at 600 °C for 16 h with an initial ramp rate of 5 °C / min, finally, the furnace was switched off to cool down to room temperature. The intermediate product was removed from the tube in the glove box, ground, and then pressed into a pellet which was introduced into the same Ta holder for further period of annealing at 300 °C for 1 h and 600 °C for 16 h with the same heating rate with 2 intermediate grindings and pelletizations to increase crystallinity.

2.2. Instrumentation

Ambient temperature high-resolution synchrotron x-ray powder diffraction (SXRPD) data of the precursors were collected with the diffractometer on beamline ID31 (λ = 0.40006 Å for K_6C_{60} and Cs_6C_{60}, and λ = 0.399838 Å for Ba_6C_{60}) at the ESRF, Grenoble, France. SXRPD data of the target compound $K_{1.5}Ba_{0.25}CsC_{60}$ were collected on beamline BL44B2 (λ = 0.500127 Å) at the SPring-8, Japan. The samples were loaded into 0.5 mm diameter glass capillaries and sealed under ~350 mbar He pressure for the SXRPD measurements.

SXRPD data were analyzed using the Rietveld refinement technique with the GSAS suite of the Rietveld programs [25]. The following procedure was applied for the Rietveld analysis: a complex peak shape function known as the pseudo-Voigt, which is a combination by addition of Gaussian and Lorentzian functions [26] was used to model the peak shape, and peak shape coefficients *GU, GV, GW, LX, LY* and *Lij* (i, j = 1–3) were refined. Low-angle peak asymmetry rising from axial divergence was modeled with coefficients S/L = 0.001, H/L = 0.0005 where L is the diffractometer radius, and H and S are the sample and detectors heights, respectively [25]; a Chebyschev polynomial function (~20 terms) was applied to fit the background; the anomalous contributions to the X-ray form factors of all atoms, f' and f" corrections to f, were calculated (in e/atom) using the program DISPANO [27] and implemented into GSAS as follows: for λ = 0.4 Åf' = 0.054, f" = 0.079 for K, f' = −1.771, f" = 0.819 for Ba and f' = −1.921, f" = 0.758 for Cs and for λ = 0.5 Å f' = 0.094, f" = 0.125 for K, f' = −1.190, f" = 1.228 for Ba and f' = −1.247, f" = 1.138 for Cs. Intermediate refinements of lattice parameters, occupancies of the tetrahedral sites, thermal parameters, peak shape coefficients, zero correction, and background function were applied during the Rietveld analysis.

3. Results

3.1. Structural characterization of the K_6C_{60}, Cs_6C_{60} and Ba_6C_{60} precursors

Rietveld refinements of the SXRPD data (Figure 1) collected for K_6C_{60}, Cs_6C_{60}, and Ba_6C_{60} confirm that samples are high quality, phase-pure, and crystallize with a body-centered-cubic structure with a space group of $Im\bar{3}$ and lattice parameters a_{K6C60} = 11.3775(2) Å, a_{Cs6C60} = 11.7887(2) Å, and a_{Ba6C60} = 11.1879(2) Å respectively. These values are in agreement with the previously-reported lattice parameters: 11.39 Å [28], 11.79 Å [29], and 11.1850(7) Å[30], respectively. This confirms that the synthesized A_6C_{60} fullerides can be used effectively as precursors. Fractional atomic coordinates of K_6C_{60}, Cs_6C_{60}, and Ba_6C_{60} were taken from [28], [29], and [31], respectively and were not refined. Only lattice constants and thermal displacement parameters, which were modeled isotopically, were refined together with instrumental (*e.g.* zero shift) and profile shape coefficients. As seen in Figure 1, a good agreement between the calculated and observed profile is obtained from the Rietveld analysis with $\chi^2 \sim 1$.

3.2. Structural characterization of the target compound $K_{1.5}Ba_{0.25}CsC_{60}$

Rietveld analysis of the X-ray diffraction data of $K_{1.5}Ba_{0.25}CsC_{60}$ readily reveals that the sample is single phase and adopts the cubic structure with fcc symmetry (Figure 2). All diffraction peaks can be indexed with the cubic structure, with no

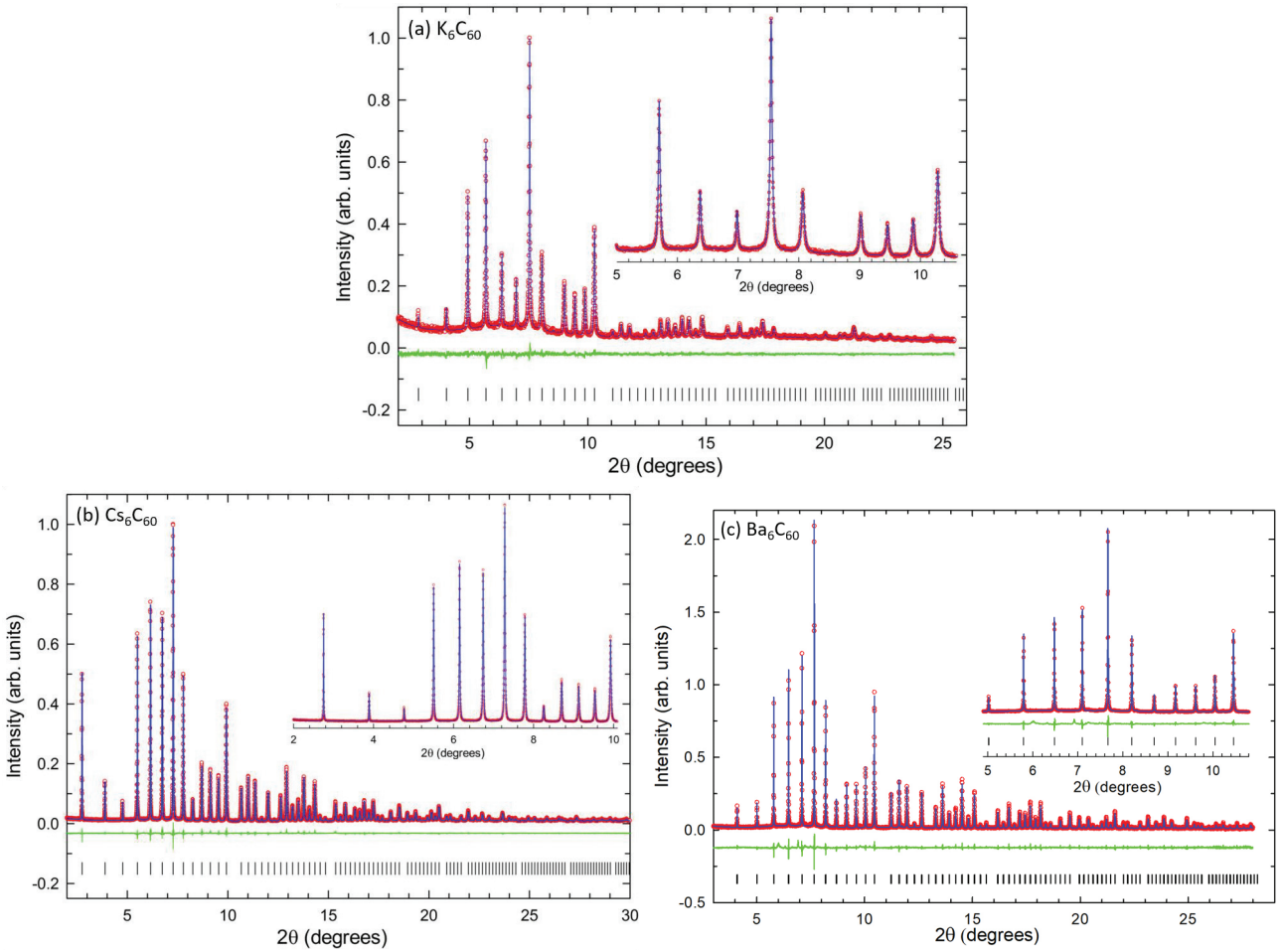

Figure 1. Rietveld fits to synchrotron XRPD data collected at ambient temperature for phase-pure (a) K_6C_{60} (λ = 0.40006 Å, R_{wp} = 4.43% and R_{exp} = 4.03%), (b) Cs_6C_{60} (λ = 0.40006 Å, R_{wp} = 4.23% and R_{exp} = 3.91%) and (c) Ba_6C_{60} (λ = 0.39984 Å, R_{wp} = 3.04% and R_{exp} = 2.20%). Red circles, blue line, and green line represent the observed, calculated, and difference profiles, respectively. Black ticks mark the reflection positions of K_6C_{60}, Cs_6C_{60} and Ba_6C_{60} ($Im\bar{3}$). Insets show expanded regions of the relevant diffraction profiles.

sign of additional reflections that could have indicated the existence of a vacancy-ordered superstructure. A merohedrally disordered fcc model with the space group of $Fm\bar{3}m$ was employed to model the fcc phase. A cation disordered model was applied as follows. As the O_h interstitial site of the fcc C_{60} structure (r = 2.06 Å) is significantly larger than the T_d one (r = 1.12 Å), larger Cs^+ ions preferentially reside in the O_h site. As a result, the O_h cavity is only occupied by Cs^+ while the smaller K^+ and Ba^{2+} ions (r_{K+} = 1.38 Å, r_{Ba2+} =1.35 Å, r_{Cs+} = 1.67 Å) preferentially occupy the T_d site. Hence, the latter is filled by a disordered mixture of K^+ and Ba^{2+}. The applicability of this method has been previously confirmed by ^{133}Cs, ^{39}K, and ^{87}Rb NMR measurements [9,32].

The fractional atomic coordinates of the fcc phase were not allowed to refine, instead they were rescaled from fcc Rb_3C_{60} (with C_{60} C-C bond distances of 1.42 Å [28]). Thermal displacement parameters of the atoms (U) were modeled isotropically and allowed to refine but under the condition that U_{iso} of the C atoms and U_{iso} of the K^+ and Ba^{2+} ions introduced into the tetrahedral site were forced to be equivalent to each other, respectively. The K^+ and Ba^{2+}occupancy in the T_d site of the fcc structure was allowed to refine but total site occupancy was fixed at 1.75, and the remaining is the vacant tetrahedral site occupancy which is 0.25. The refined occupancy ratio converged to K^+: Ba^{2+} = 0.712(10):0.163(10) leading to a refined composition of $K_{1.42(1)}Ba_{0.33(1)}CsC_{60}$. The structural parameters of the fcc phase obtained from the Rietveld refinement are summarized in Table.

Indeed, substitution of smaller Ba^{2+} for the K^+ cation, and the presence of the T_d vacancy in fcc $K_xCs_{3-x}C_{60}$ led to a significant lattice contraction. The fcc lattice parameter of refined composition $K_{1.42(1)}Ba_{0.33(1)}CsC_{60}$,*a,* is obtained as 14.2616(1) Å, which is smaller than those of any $K_xCs_{3-x}C_{60}$ ternary compositions (Figure 3), covering the compositional

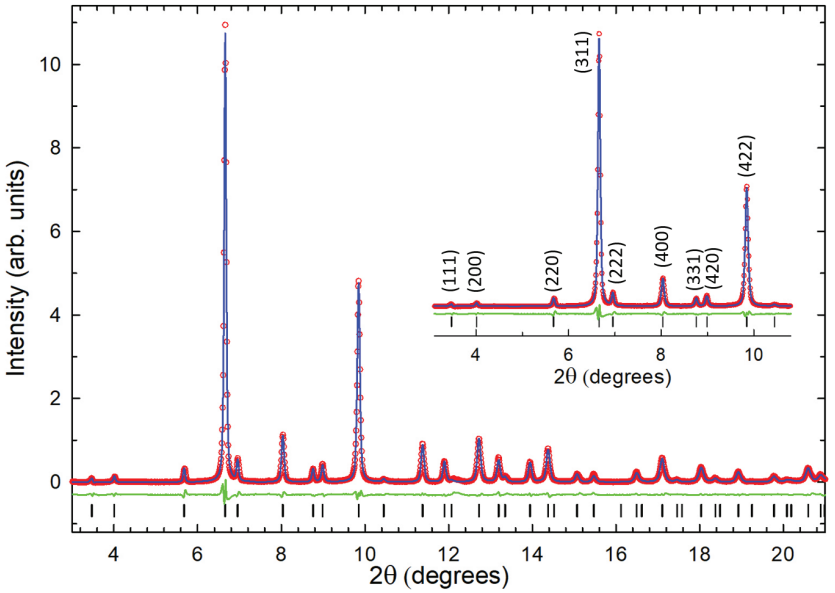

Figure 2. Rietveld fits to synchrotron XRPD data collected at ambient temperature for phase-pure fcc $K_{1.5}Ba_{0.25}CsC_{60}$ (λ = 0.500127 Å, R_{wp} = 2.76% and R_{exp} = 1.29%). Red circles, blue line, and green line represent the observed, calculated, and difference profiles, respectively. Black ticks mark the reflection positions of fcc phase (space group $Fm\bar{3}m$). The inset shows an expanded region of the diffraction profile with observed Bragg peaks labeled with their (hkl) Miller indices.

Table. Refined structural parameters for fcc-structured $K_{1.5}Ba_{0.25}CsC_{60}$ (refined composition $K_{1.42(1)}Ba_{0.33(1)}CsC_{60}$) from Rietveld analysis of SXRPD data collected at ambient temperature, with λ = 0.500127 Å. Site multiplicities and occupancies are listed in columns *M* and *N*, respectively. Values in parentheses are estimated errors from the least-squares fitting. The weighted-profile and expected *R*-factors are R_{wp} = 2.76%, and R_{exp} = 1.29%, respectively. The lattice constant is *a* = 14.2616(1) Å.

	x/*a*	*y*/*b*	*z*/*c*	*M*	*N*	U_{iso} (10² Å²)
K	0.25	0.25	0.25	8	0.712(3)	1.8(1)
Ba	0.25	0.25	0.25	8	0.163(3)	1.8(1)
Cs	0.5	0.5	0.5	4	1.0	7.8(1)
C(1)	0	0.04985	0.24176	96	0.5	0.6(1)
C(2)	0.21102	0.08059	0.09949	192	0.5	0.6(1)
C(3)	0.18008	0.16107	0.04989	192	0.5	0.6(1)

range 0.22(1) ≤ x ≤ 2 and lattice constants14.28571(7) Å ≤ *a* ≤ 14.7011(2) Å [32]. This reflects the fact that the average ionic radii of the cations residing in the T_d and O_h cavities, $\langle r_A \rangle$ in $K_{1.42(1)}Ba_{0.33(1)}CsC_{60}$ is smaller, $\langle r_A \rangle$= 1.36(1) Å, than that of any $K_xCs_{3-x}C_{60}$ compositions (1.38 Å ≤ $\langle r_A \rangle$ ≤ 1.64(1) Å). Refined isotropic thermal displacement parameters of the cations occupying the T_d and O_h cavities, and also of the C atoms are found to be in good agreement with those known from the literature[12]. Because of the smaller size of the T_d site compared with the O_h one, thermal displacements of the atoms residing in the former one is expected to be relatively smaller than the ones in the latter.

4. Discussion

The molecular, alkali doped A_3C_{60} fulleride family possesses remarkable physical properties (e.g. unconventional superconductivity, and strong electron correlations) originating from their molecular electronic structure which can

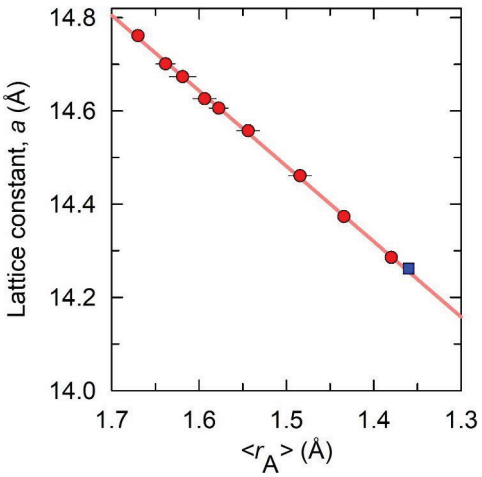

Figure 3. Variation of the ambient temperature fcc lattice constant of $K_{1.5}Ba_{0.25}CsC_{60}$ (blue square) and $K_xCs_{3-x}C_{60}$ ($0 \le x \le 2$, red circles, data taken from [32]) with average ionic radii of the cations residing in the T_d and O_h cavities, $\langle r_A \rangle$. The solid line through data points is a linear fit, yielding a value of $da/d\langle r_A \rangle = -1.61(1)$ Å.

be easily tuned via physical/chemical pressure and temperature without altering their high fcc symmetry. The donor intercalants in molecular fulleride family possessing unique properties are not only limited to alkali and alkaline earth metals, for example, rare-earth doped $Yb_{2.75}C_{60}$ fulleride becomes superconducting below 6 K and shows an exceptional crystal structure contrary to the literature [24]. In a hypothetical Yb_3C_{60}, Yb cations reside at the centers of the O_h and T_d sites of the fcc C_{60} lattice. However, in $Yb_{2.75}C_{60}$,Yb cations occupy off-centered interstitial sites and leave one out of every eight T_d sites vacant. These vacancy sites display long-range ordering, generating a new cation-vacancy-ordered superstructure, which leads to a unit cell with dimensions twice as large as those of the common fcc fulleride structures [24]. A similar situation is also encountered in $Sm_{2.75}C_{60}$ [23]. In both cases, their complex structure arises from the long-range ordering of tetrahedral rare-earth metal vacancies. In this study, we also aimed to induce such structural response to the presence of vacancy site in $K_{1.42(1)}Ba_{0.33(1)}CsC_{60}$, however, this could not be achieved. Inspection of the diffraction profile did not reveal any superlattice peaks at low angles that could be indexed to an enlarged unit cell, which may possibly signify the generation of a superstructure as in $Sm_{2.75}C_{60}$ and $Yb_{2.75}C_{60}$. The underlying physical origin of this type of vacancy-ordering was attributed to a strong directional interaction between electron-poor, charge-deficient five-membered rings of C_{60} and divalent ytterbium cations but not to the cation size difference [24]. However, this suggestion might not be valid in the case of using larger cations as in the present study, i.e. K^+(1.38Å), and Ba^{2+}(1.35 Å), than that of the tetrahedral hole (1.12Å) but the ionic radius of Yb^{2+} and Sm^{2+} are 1.02 and 1.14 Å, respectively, comparable to that of the tetrahedral hole. As it is well known, the size and amount of the dopant species has a primary effect on the crystal structure of fullerides, for instance, contrary to the literature, at low temperatures, the structure of Na_2CsC_{60}(r_{Na+} = 1.02 Å) is primitive cubic ($Pa\bar{3}$) being isostructural with pristine C_{60} and undergoes a phase transition on heating to an fcc phase with a space group of $Fm\bar{3}m$ [33], and the structure of $Yb_{2.75}C_{60}$ is orthorhombic with space group *Pcab* [24]. Therefore, it could be tentatively suggested that the size of the cations residing in the tetrahedral site should be taken into account if one aims to generate a long-range arrangement of vacant sites, namely a superstructure.

5. Conclusion

In conclusion, the preparation of the nominal $K_{1.5}Ba_{0.25}CsC_{60}$ fulleride using stoichiometric quantities of K_6C_{60}, Cs_6C_{60}, and Ba_6C_{60} precursors, which overcomes inadequate stoichiometry control, via solid-state synthetic route is presented. Structural characterization of the precursors and the target compound was performed with Rietveld analysis of the high-resolution synchrotron X-ray powder diffraction data. The analysis confirmed that the structure of the precursors is body-centered-cubic ($Im\bar{3}$) as reported in the literature and free from impurity phases such as oxides of the metals which can be easily formed during the synthetic protocol applied.

The X-ray diffraction pattern of the target compound $K_{1.5}Ba_{0.25}CsC_{60}$ (refined composition: $K_{1.42(1)}Ba_{0.33(1)}CsC_{60}$) has shown no evidence for the emergence of superstructure peaks which could have resulted from the long-range ordering of the vacant tetrahedral sites. All the Bragg reflections existing in the diffraction pattern originate from the cubic structure ($Fm\bar{3}m$) without any violation. This suggests that there is no long-range ordered arrangement of tetrahedral alkaline-earth

metal vacancies in $K_{1.42(1)}Ba_{0.33(1)}CsC_{60}$. The reason for this could be the use of highly symmetric Cs_3C_{60} fulleride as a parent phase and of moderately large dopant species, i.e. K^+, Ba^{2+}. This issue merits more detailed investigation through the synthesis and characterization of vacancy-doped fullerides with lower symmetry, for instance, primitive cubic Na_2CsC_{60} could be gradually substituted nonstoichiometrically by a smaller divalent cation which might generate ordering of cation-vacancy and also noninteger valence of C_{60}.

Acknowledgment
The author would like to express sincere thanks to K. Prassides and R. H. Colman for their assistance and discussion, and thanks the beamline scientists A. Fitch at the ESRF and K. Kato at the SPring-8 for their help during the measurements. The author also thanks the ESRF and SPring-8 for access to synchrotron X-ray facilities.

References

1. Dresselhaus MS, Dresselhaus G, Eklund PC. Science of Fullerenes and Carbon Nanotubes. Academic Press, 1996.
2. Haddon RC, Hebard AF, Rosseinsky MJ, Murphy DW, Duclos SJ, et al. Conducting films of C_{60} and C_{70} by alkali-metal doping. Nature 1991; 350 (6316): 320-322. doi: org/10.1038/350320a0
3. Hebard AF, Rosseinsky MJ, Haddon RC, Muphy DW, Glarum SH, et al. Superconductivity at 18 K in potassium-doped C_{60}. Nature 1991; 350: 600-601. doi: 10.1038/350600a0
4. Holczer K, Klein O, Huang SM, Kaner RB, Fu KJ, et al. Alkali-Fulleride Superconductors: Synthesis, Composition, and Diamagnetic Shielding. Science 1991; 252 (5009): 1154-1157. doi:10.1126/science.252.5009.1154
5. Stephens PW, Mihaly L, Lee PL, Whetten R. L, Huang SM, et al. Structure of single-phase superconducting K_3C_{60}. Nature 1991; 351: 632-634. doi:10.1038/351632a0
6. Rosseinsky MJ, Ramirez AP, Glarum SH, Murphy DW, Haddon RC, et al. Superconductivity at 28 K in Rb_xC_{60}. Physical Review Letters 1991; 66 (21): 2830-2832. doi:10.1103/PhysRevLett.66.2830
7. Tanigaki K, Ebbesen TW, Saito S, Mizuki J, Tsai JS, et al. Superconductivity at 33 K in $Cs_xRb_yC_{60}$. Nature 1991; 352: 222-223. doi:10.1038/352222a0
8. Ganin AY, Takabayashi Y, Jeglič P, Arčon D, Potočnik A, et al. Polymorphism control of superconductivity and magnetism in Cs_3C_{60} close to the Mott transition. Nature 2010; 466: 221-227. doi: 10.1038/Nature09120
9. Zadik RH, Takabayashi Y, Klupp G, Colman RH, Ganin AY, et al. Optimized unconventional superconductivity in a molecular Jahn-Teller metal. Science Advances 2015; 1 (3): e1500059. doi:10.1126/sciadv.1500059
10. Takabayashi Y, Ganin AY, Jeglic P, Arčon D, Takano T, et al. The disorder-free non-BCS superconductor Cs_3C_{60} emerges from an antiferromagnetic insulator parent state. Science 2009; 323 (5921): 1585-1590. doi:10.1126/science.1169163
11. Menelaou M, Takabayashi Y, Okur HE, Zadik RH, Prassides K. Structural and electronic response of overexpanded superconducting fullerides close to the Mott insulator boundary. International Journal of Modern Physics B 2018; 32 (17): 1840020. doi:10.1142/S0217979218400209
12. Okur HE, Prassides K. Structural and electronic properties of the overexpanded quaternary superconducting fulleride $K_{0.25}Rb_{0.25}Cs_{2.5}C_{60}$. Journal of Physics and Chemistry of Solids 2019; 131: 44-49. doi:10.1016/J.JPCS.2019.03.017
13. Wzietek P, Mito T, Alloul H, Pontiroli D, Aramini M, Ricco M. NMR Study of the Superconducting Gap Variation near the Mott Transition in Cs_3C_{60}. Physical Review Letters 2014; 112 (6): 066401. doi:10.1103/PhysRevLett.112.066401
14. Alloul H, Wzietek P, Mito T, Pontiroli D, Aramini M, et al. Mott Transition in the A15 Phase of Cs_3C_{60}: Absence of a Pseudogap and Charge Order. Physical Review Letters 2017; 118 (23): 237601. doi:10.1103/PhysRevLett.118.237601
15. Potočnik A, Ganin AY, Takabayashi Y, McDonald MT, Heinmaa I, et al. Jahn-Teller orbital glass state in the expanded fcc Cs_3C_{60} fulleride. Chemical Science 2014; 5 (8): 3008-3017. doi:10.1039/c4sc00670d
16. Potočnik A, Krajnc A, Jeglič P, Takabayashi Y, Ganin AY, et al. Size and symmetry of the superconducting gap in the f.c.c. Cs_3C_{60} polymorph close to the metal-Mott insulator boundary. Scientific Reports 2014; 4: 4265. doi:10.1038/srep04265
17. Kasahara Y, Takeuchi Y, Itou T, Zadik RH, Takabayashi Y, et al. Spin frustration and magnetic ordering in the S = 1/2 molecular antiferromagnet fcc - Cs_3C_{60}. Phys. Rev. B 2014; 90 (1): 14413-14419 doi:10.1103/PhysRevB.90.014413
18. Ihara Y, Alloul H, Wzietek P, Pontiroli D, Mazzani M, Riccò M. NMR Study of the Mott Transitions to Superconductivity in the Two Cs_3C_{60} Phases. Physical Review Letters 2010; 104 (25): 256402.doi:10.1103/PhysRevLett.104.256402

19. Klupp G, Matus P, Kamarás K, Ganin AY, McLennan A, et al. Dynamic Jahn-Teller effect Mott Transitions to Superconductivity in the Two in the parent insulating state of the molecular superconductor Cs_3C_{60}. Nature Communications 2012; 3 (912). doi: 10.1038/Ncomms1910

20. Kamarás K, Klupp G, Matus P, Ganin AY, McLennan A, et al. Mott localization in the correlated superconductor Cs_3C_{60}resulting from the molecular Jahn-Teller effect. Journal of Physics: Conference Series 2013; 428 (1): 012002. doi:10.1088/1742-6596/428/1/012002

21. Fleming RM, Ramirez AP, Rosseinsky MJ, Murphy DW, Haddon RC, et al. Relation of structure and superconducting transition temperatures in A_3C_{60}. Nature 1991; 352 (6338): 787-788. doi:10.1038/352787a0

22. McCauley JP, Zhu Q, Coustel N, Zhou O, Vaughan G, et al. Synthesis, Structure and Superconducting Properties of Single-Phase Rb3C60. A New, Convenient Method for the Preparation of M_3C_{60} Superconductors. Journal of the American Chemical Society 1991; 113 (22): 8537-8538. doi:10.1021/ja00022a060

23. Arvanitidis J, Papagelis K, Margadonna S, Prassides K, Fitch AN. Temperature-induced valence transition and associated lattice collapse in samarium fulleride. Nature 2003; 425 (6958): 599-602. doi:10.1038/nature01994

24. Özdaş E, Kortan AR, Kopylov N, Ramirez AP, Siegrist T, et al. Superconductivity and cation-vacancy ordering in the rare-earth fulleride $Yb_{2.75}C_{60}$. Nature 1995; 375 (6527): 126-129. doi:10.1038/375126a0

25. Larson AC, Von Dreele R. General Structure Analysis System (GSAS). Los Alamos National Laboratory Report LAUR 2004: 86-748.

26. Young RA, Wiles DB. Profile shape functions in Rietveld refinements. Journal of Applied Crystallography 1982; 15 (4): 430-438. doi:10.1107/S002188988201231X

27. Laugier J, Bochu B. LMGP-Suite of Programs for the interpretation of X-ray Experiments. 1999.

28. Zhou O, Cox D. Structures of C_{60} intercalation compounds. Journal of Physics and Chemistry of Solids 1992; 53 : 1373-1390. doi:10.1016/0022-3697(92)90233-4

29. Zhou O, Fischer JE, Coustel N, Kycia S, Zhu Q, et al. Structure and bonding in alkali-metal-doped C_{60}. Nature 1991; 351 (6326): 462-464. doi:10.1038/351462a0

30. Gogia B, Kordatos K, Suematsu H, Tanigaki K, Prassides K. Electronic states of Ba_6C_{60} and Sr_6C_{60} fullerides. Physical Review B 1998; 58 : 1077-1079. doi:10.1103/PhysRevB.58.1077

31. Kortan AR, Kopylov N, Glarum S, Gyorgy EM, Ramirez AP, et al. Superconductivity in Barium Fulleride. Nature 1992; 360: 566-568. doi:10.1038/360566a0

32. Okur HE. Experimental Investigations of Correlated Electron Systems: Alkali Fullerides and Sesquioxides. PhD, Durham University, Durham, UK, 2016.

33. Prassides K, Christides C, Thomas IM, Mizuki J, Tanigaki K, et al. Crystal Structure, Bonding and Phase Transition of the Superconducting Na_2CsC_{60} Fulleride. Science 1994; 263 (5149): 950-954. doi:10.1126/science.263.5149.950